Atmos. Chem. Phys. Discuss., 14, 17635–17679, 2014
www.atmos-chem-phys-discuss.net/14/17635/2014/
doi:10.5194/acpd-14-17635-2014

Atmospheric Chemistry and Physics Discussions

Effects of preexisting ice crystals on cirrus clouds and comparison between different ice nucleation parameterizations with the Community Atmosphere Model (CAM5)

X. Shi[1,2,3], **X. Liu**[1], **and K. Zhang**[4]

[1]Department of Atmospheric Science, University of Wyoming, Laramie, WY, USA
[2]Hebei Key Laboratory for Meteorology and Eco-environment, Shijiazhuang, China
[3]Hebei Climate Center, Shijiazhuang, China
[4]Atmospheric Science and Global Change Division, Pacific Northwest National Laboratory, Richland, WA, USA

Received: 12 June 2014 – Accepted: 23 June 2014 – Published: 2 July 2014

Correspondence to: X. Liu (xliu6@uwyo.edu)

Published by Copernicus Publications on behalf of the European Geosciences Union.

Abstract

In order to improve the treatment of ice nucleation in a more realistic manner in the Community Atmospheric Model version 5.3 (CAM5.3), the effects of preexisting ice crystals on ice nucleation in cirrus clouds are considered. In addition, by considering the in-cloud variability in ice saturation ratio, homogeneous nucleation takes place spatially only in a portion of cirrus cloud rather than in the whole area of cirrus cloud. With these improvements, the two unphysical limiters used in the representation of ice nucleation are removed. Compared to observations, the ice number concentrations and the probability distributions of ice number concentration are both improved with the updated treatment. The preexisting ice crystals significantly reduce ice number concentrations in cirrus clouds, especially at mid- to high latitudes in the upper troposphere (by a factor of ~ 10). Furthermore, the contribution of heterogeneous ice nucleation to cirrus ice crystal number increases considerably.

Besides the default ice nucleation parameterization of Liu and Penner (2005, hereafter LP) in CAM5.3, two other ice nucleation parameterizations of Barahona and Nenes (2009, hereafter BN) and Kärcher et al. (2006, hereafter KL) are implemented in CAM5.3 for the comparison. In-cloud ice crystal number concentration, percentage contribution from heterogeneous ice nucleation to total ice crystal number, and preexisting ice effects simulated by the three ice nucleation parameterizations have similar patterns in the simulations with present-day aerosol emissions. However, the change (present-day minus pre-industrial times) in global annual mean column ice number concentration from the KL parameterization ($3.24 \times 10^6\,\mathrm{m}^{-2}$) is obviously less than that from the LP ($8.46 \times 10^6\,\mathrm{m}^{-2}$) and BN ($5.62 \times 10^6\,\mathrm{m}^{-2}$) parameterizations. As a result, experiment using the KL parameterization predicts a much smaller anthropogenic aerosol longwave indirect forcing ($0.24\,\mathrm{W\,m}^{-2}$) than that using the LP ($0.46\,\mathrm{W\,m}^{-2}$) and BN ($0.39\,\mathrm{W\,m}^{-2}$) parameterizations.

ACPD
14, 17635–17679, 2014

1 Introduction

Cirrus clouds play an import role in the global climate system because they have extensive global coverage (Wang et al., 1996; Wylie and Menzel, 1999). They cool the planet by reflecting the solar radiation back to space and on other hand heat the planet by absorbing and re-emitting the longwave terrestrial radiation (Liou, 1986; Rossow and Schiffer, 1999; Chen et al., 2000; Corti et al., 2005). The balance of these two processes depends mainly on cirrus optical properties and thus on ice crystals number concentration (Haag, 2004; Kay et al., 2006; Fusina et al., 2007; Gettelman et al., 2012). Furthermore, the microphysical properties of cirrus clouds strongly influence the efficiency of dehydration at the tropical tropopause layer and then modulate water vapor in the upper troposphere and lower stratosphere (Korolev and Isaac, 2006; Krämer et al., 2009; Jensen et al., 2013).

Although cirrus clouds are an important player in the global climate system, the current knowledge of cirrus clouds formation is still in its infancy (Heymsfield et al., 2005; Jensen et al., 2010; Murray et al., 2010; Barahona and Nenes, 2011; Cziczo et al., 2013; Spichtinger and Krämer, 2013). Ice crystals may form by both homogeneous freezing of soluble aerosol/droplet particles and heterogeneous ice nucleation on insoluble aerosol particles, called ice nuclei (IN, Pruppacher and Klett, 1997). Various insoluble or partly insoluble aerosol particles can act as IN (Szyrmer and Zawadzki, 1997; DeMott et al., 2000; Cziczo et al., 2004; Phillips et al., 2008; Murray et al., 2010). Understanding the role of different aerosol types in heterogeneous ice nucleation remains enigmatic (Kärcher et al., 2007; DeMott et al., 2011). Compared to heterogeneous nucleation, homogeneous nucleation is relatively better understood (Koop et al., 2000; Koop, 2004). The number concentration of soluble aerosol particles in the upper troposphere is usually much higher than that of IN. Once taking place, homogeneous freezing can generate a high number concentration of ice crystals in cold environments with high updraft velocities, and has been assumed to be a dominant process for cirrus cloud formation (Heymsfield et al., 2005; Wang and Penner,

ACPD
14, 17635–17679, 2014

2010; Gettelman et al., 2012). However, heterogeneous nucleation tends to occur at lower supersaturations, depletes the water vapor, and thus prevents the homogeneous nucleation from occurring or reduce the number of ice crystals produced by the homogeneous freezing (Kärcher and Lohmann, 2003; Spichtinger and Gierens, 2009). The relative contribution of homogeneous nucleation vs. heterogeneous nucleation to cirrus cloud formation is uncertain (Jensen et al., 2012; Zhang et al., 2013a). Aircraft measurements over North and Central America and nearby oceans indicate that heterogeneous freezing might be the dominant formation mechanism and the occurrence frequency of homogeneous nucleation is very low by analyzing ice residues collected in these cirrus clouds (Cziczo et al., 2013). However, simulations from general circulation models (GCM) with physically-based ice nucleation parameterizations often show that homogeneous freezing is the primary contributor to ice number concentration in cirrus clouds (Lohmann et al., 2008; Liu et al., 2012a; Kuebbeler et al., 2014).

Aerosol indirect effects on cloud properties are one of the largest uncertainties in the projection of future climate change (Lohmann and Feichter, 2005; IPCC, 2007). There have been significant progresses in recent years in developing ice microphysics schemes for GCMs and studying aerosol effects on cirrus clouds (Liu et al., 2007; Gettelman et al., 2010; Salzmann et al., 2010; Wang and Penner, 2010; Hendricks et al., 2011; Barahona et al., 2013; Shi et al., 2013; Kuebbeler et al., 2014). The root of aerosol indirect effects on cirrus clouds is to link ice number concentrations to aerosol properties and environmental conditions (e.g., temperature and updraft velocity). Based on theoretical formulations or model simulations of the ice crystal formation process in a rising air parcel, sophisticated ice nucleation parameterizations considering the competition between homogeneous and heterogeneous nucleation have been developed (Liu and Penner, 2005; Kärcher et al., 2006; Barahona and Nenes, 2009). Compared to the two parameterizations of Liu and Penner (2005, hereafter LP) and Barahona and Nenes (2009, hereafter BN), the parameterization of Kärcher et al. (2006, hereafter KL) takes the effects of preexisting ice crystals (PREICE) on ice nucleation into account. The presence of PREICE prior to ice nucleation events hinders

ACPD
14, 17635–17679, 2014

homogeneous and heterogeneous nucleation from happening owing to the depletion of water vapor on PREICE. Simulation results from the European Centre Hamburg model (ECHAM) with the KL parameterization showed that the PREICE effects lead to cirrus clouds composed of fewer and larger ice crystals (Hendricks et al., 2011; Kuebbeler et al., 2014). Barahona et al. (2013) incorporated the BN parameterization into the NASA Goddard Earth Observing System model version 5 (GEOS5), and modified the original BN parameterization to include the PREICE effects. Model results showed that cloud forcings are significantly reduced due to the effects of PREICE.

In this study, the LP parameterization used for ice nucleation in the default CAM5, the atmospheric component of the Community Earth System Model (CESM), is modified to consider the PREICE effects. Furthermore, the occurrence probability of homogeneous freezing events in cirrus clouds is derived and implemented in CAM5 by including the in-cloud variability of ice saturation ratio. Model simulations with the modified LP parameterization are compared to observations to examine the performance of model. In addition, we implemented BN and KL parameterizations in CAM5 to investigate the comparison between different ice nucleation parameterizations. This paper is organized as follows. Model description is presented in Sect. 2. Model simulations are evaluated and compared with observations in Sect. 3. Section 4 examines the effects of PREICE. Section 5 presents the comparison between different ice nucleation parameterizations. Conclusions are given in Sect. 6.

2 CAM model and experiments

2.1 Cirrus cloud scheme in CAM5

The model used in this study is the version of CAM5.3 (Neale et al., 2012). The treatment of clouds in CAM5.3 is divided into two categories: highly parameterized convective cloud scheme and relatively detailed stratiform cloud scheme. Convective microphysics does not consider the effects of aerosol particles on convective cloud droplets

ACPD
14, 17635–17679, 2014

and ice crystals. A two-moment stratiform cloud microphysics scheme (Morrison and Gettelman, 2008, hereafter MG; Gettelman et al., 2008, 2010) has been implemented in CAM5.3, which is also coupled to a modal aerosol module (Liu et al., 2012b) for aerosol-cloud interactions. The default three-mode version of the modal aerosol module, which consists of Aitken, accumulation and coarse modes, is used in this study. Ice crystals in cirrus clouds form through the homogenous freezing of sulfate particles in the Aitken mode and heterogeneous nucleation on dust particles in the coarse mode in CAM5 (Gettelman et al., 2010). Cloud water from the convective detrainment at temperatures below −30 °C is assumed to be cloud ice with a prescribed mean radius (Gettelman et al., 2010). The ice cloud fraction is diagnosed using the total water (water vapor and cloud ice), based on Gettelman et al. (2010). Considering the increase in cloud ice mixing ratio due to vapor deposition during one time step, the growth of ice crystals is calculated using a relaxation timescale (Morrison and Gettelman, 2008; Gettelman et al., 2010). Supersaturation with respect to ice is allowed in the model, and grid-mean relative humidity with respect to ice (RH_i) is used in the calculation of deposition growth of ice crystals (Liu et al., 2007; Gettelman et al., 2010).

2.2 Ice nucleation parameterization in the standard CAM5

Ice nucleation for cirrus clouds in CAM5 is based on the LP parameterization, which includes the competition between homogeneous nucleation on sulfate and heterogeneous nucleation (immersion freezing) on dust. LP parameterization is derived from fitting the simulation results of a cloud parcel with constant updraft velocities. The number of nucleated ice crystals is a function of relative humidity, temperature, aerosol number concentration, and updraft velocity. Since the current CAM5 model grid cannot resolve the sub-grid scale variability of vertical velocity, W_{sub}, it is diagnosed from the square root of the turbulent kinetic energy calculated in the moisture turbulence parameterization in CAM5.3 (Bretherton and Park, 2009). An upper limit of $0.2\,m\,s^{-1}$ is assumed for W_{sub} to fit to the observed ice number concentrations (Gettelman et al., 2010). Dust in the coarse aerosol mode is taken as potential heterogeneous IN. Homo-

ACPD
14, 17635–17679, 2014

geneous nucleation uses the sulfate aerosol particles in the Aiken mode with diameter greater than 0.1 µm. The purpose of using this size limiter is also to fit to the observed ice number concentrations (Gettelman et al., 2010). Unlike the cloud droplet activation in warm liquid-phase clouds that occurs in all levels of new clouds or at the cloud base of old clouds in CAM5, ice nucleation parameterization for cirrus clouds is applied in all cloud levels because ice nucleation can happen in cirrus clouds where ice supersaturations can occur frequently (Krämer et al., 2009). The ice number concentration calculated from the ice nucleation parameterization, N_{aai}, is assumed to be the maximum in-cloud ice number concentration under the current condition. New ice crystals will be produced if the current in-cloud ice number concentration, N_i, falls below N_{aai}. This is described in Eq. (1) as

$$\frac{dN_i}{dt} = \max\left(0, \frac{N_{aai} - N_i}{dt}\right). \quad (1)$$

2.3 Effects of PREICE on ice nucleation

Physically-based ice nucleation parameterizations are developed from the theoretical formulations that describe the cirrus cloud initiation process in an adiabatic rising air parcel. Without the PREICE effect, the temporal evolution of the ice saturation ratio, S_i, is governed by (Kärcher et al., 2006)

$$\frac{dS_i}{dt} = a_1 S_i W - (a_2 + a_3 S_i)\frac{dq_{i,nuc}}{dt}, \quad (2)$$

where the parameters a_1, a_2, and a_3 depend only on the ambient temperature (T) and pressure (P), W is the updraft velocity, and $\frac{dq_{i,nuc}}{dt}$ denotes the growth rate of newly-nucleated ice crystals. To account for the PREICE effects, the depositional growth of PREICE, $\frac{dq_{i,pre}}{dt}$ is added to Eq. (2)

$$\frac{dS_i}{dt} = a_1 S_i W - (a_2 + a_3 S_i)\left(\frac{dq_{i,nuc}}{dt} + \frac{dq_{i,pre}}{dt}\right). \quad (3)$$

ACPD
14, 17635–17679, 2014

Equation (3) can be rewritten in the following form

$$\frac{dS_i}{dt} = a_1 S_i (W - W_{i,pre}) - (a_2 + a_3 S_i) \frac{dq_{i,nuc}}{dt}, \quad (4)$$

$$W_{i,pre} = \frac{a_2 + a_3 S_i}{a_1 S_i} \frac{dq_{i,pre}}{dt}. \quad (5)$$

Compared to Eq. (2), Eq. (4) indicates that the PREICE effect can be parameterized by reducing the vertical velocity for ice nucleation. This vertical velocity reduction, $W_{i,pre}$, caused by PREICE is calculated by Eq. (5).

Assuming all preexisting ice crystals have the same radius ($R_{i,pre}$), their growth rate is given by

$$\frac{dq_{i,pre}}{dt} = \frac{4\pi\rho_i}{m_w} n_{i,pre} R_{i,pre}^2 \frac{b_1}{1 + R_{i,pre} b_2}, \quad (6)$$

where $n_{i,pre}$ is the PREICE number concentration, ρ_i is ice density, m_w is the mass of a water molecule. $b_1 = \alpha v_{th} n_{sat}(S_i - 1)/4$, $b_2 = \alpha v_{th}/(4D)$, α is the water vapor deposition coefficient on ice, v_{th} is their thermal speed, n_{sat} is the water vapor number density at ice saturation, D is the water vapor diffusion coefficient from the gas to ice phase.

Figure 1 shows $W_{i,pre}$ as a function of PREICE number concentration calculated using Eq. (5) at the homogeneous freezing saturation threshold (S_{hom}) and heterogeneous freezing saturation threshold (S_{het}). S_{hom} is a function of temperature (Kärcher and Lohmann, 2002a, b), and is 1.53 at $T = -60^{\circ}$C. For immersion freezing of coated dust particles, S_{het} varies between 1.15 and 1.7 (Hoose and Möhler, 2012; Kuebbeler et al., 2014). Here, S_{het} is assumed to be 1.3. Under conditions of $n_{i,pre} > 50\,L^{-1}$ and $R_{i,pre} > 25\,\mu m$, $W_{i,pre}$ is larger than $0.2\,m\,s^{-1}$ for homogeneous freezing. CAM5.3 model results show that nearly half of W_{sub} is less than $0.2\,m\,s^{-1}$ (Sect. 3). In the other words, the presence of PREICE prior to a new nucleation event can significantly prevent the homogeneous nucleation from happening.

ACPD
14, 17635–17679, 2014

In the MG scheme, ice crystals are assumed to follow a gamma size distribution (Morrison and Gettelman, 2008). Thus, the effective radii ($R_{\mathrm{ieff,pre}}$) is used to account for the PREICE size distribution. Because $R_{\mathrm{i,pre}} \cdot b_2$ in Eq. (6) is usually far greater than 1 (not shown), $\frac{\mathrm{d}q_{\mathrm{i,pre}}}{\mathrm{d}t}$ is proportional to the first order of $R_{\mathrm{i,pre}}$. Therefore, the $R_{\mathrm{ieff,pre}}$ used in Eq. (6) is obtained directly by using the first moment of ice particle size distribution ($0.5/\lambda$, λ is the slope parameter of Eq. (1) in Morrison and Gettelman, 2008), which is different from the effective radii needed by the radiative transfer scheme that are calculated by dividing the third and second moment of size distribution. After rearranging term (Eq. 3 in Morrison and Gettelman, 2008), this yields

$$R_{\mathrm{ieff,pre}} \cong \frac{1}{2}\left(\frac{q_{\mathrm{i,pre}}}{\pi \rho_{\mathrm{i}} n_{\mathrm{i,pre}}}\right)^{1/3}. \quad (7)$$

Figure 2 shows the schematic diagram of cirrus cloud evolution and the impact of PREICE. In the default CAM5 that neglects the PREICE effect, ice number produced from the previous ice nucleation event is 2000 L^{-1} (time step t_1). Due to sedimentation of ice crystals (and/or other sink processes), N_{i} is reduced to 1800 L^{-1}. Under the same ambient environmental conditions, N_{i} is increased back to 2000 L^{-1} at the next time step (t_2) according to Eq. (1). In the updated ice nucleation scheme, because the PREICE effect is considered, ice nucleation will not happen until Ni is reduced from 2000 L^{-1} to 50 L^{-1} at t_n. After this moment, the PREICE number ($< 50\,\mathrm{L}^{-1}$) is too low to prevent ice nucleation, so ice nucleation occurs at t_{n+1}. Note that the newly-formed ice crystals number concentration is 1500 L^{-1} instead of 2000 L^{-1} because of the presence of PREICE with the number concentration of 50 L^{-1}. Here the total N_{i} is the number concentration of newly-formed ice crystals (1500 L^{-1}) plus the number concentration of PREICE (50 L^{-1}).

ACPD
14, 17635–17679, 2014

2.4 Modifications to the standard ice nucleation parameterization in CAM5

In addition to the consideration of PREICE effects in the LP parameterization, several other modifications have been made in the ice nucleation scheme. Firstly, the lower size limiter (0.1 μm diameter) of sulfate particles used for homogeneous freezing is removed. We use the number concentration of all sulfate aerosol particles in the Aiken mode as an input for homogeneous nucleation. This is consistent with the LP parameterization, which is derived for the background sulfate aerosol particles with a lognormal size distribution. Secondly, the upper limiter ($0.2\,\mathrm{m\,s^{-1}}$) of W_{sub} is also removed because updraft velocities measured from several aircraft campaigns show frequent occurrence of larger values ($>0.2\,\mathrm{m\,s^{-1}}$, Zhang et al., 2013b). Ice crystal number concentration from homogeneous freezing is very sensitive to updraft velocity, whereas heterogeneous nucleation is not (Liu and Penner, 2005). Therefore, removing this limiter will increase the relative contribution of homogeneous nucleation to total ice crystals number. Finally, in-situ observations of cirrus clouds show that only a small fraction of in-cloud S_{i} data surpass S_{hom} (Diao et al., 2013), and this agrees with the finding that the occurrence frequency of homogeneous freezing could be significantly lower than that of heterogeneous freezing (Cziczo et al., 2013). So we assume that homogeneous freezing takes place spatially only in a portion of cirrus clouds. The in-cloud S_{i} variability can be calculated from the temperature standard deviation, δ_T, following Kärcher and Burkhardt (2008):

$$S_{\mathrm{i}}(T') \cong S_0 \exp\left[\frac{(T_0 - T')\theta}{T_0^2}\right], \tag{8}$$

$$\frac{\mathrm{d}P_{T'}}{\mathrm{d}T'} = \frac{1}{\delta_T}\frac{1}{\sqrt{2\pi}}\exp\left[-\frac{(T_0 - T')^2}{2\delta_T^2}\right], \tag{9}$$

where T_0 and S_0 are mean temperature and ice saturation, T' and $S_{\mathrm{i}}(T')$ represents local in-cloud quantities, $\frac{\mathrm{d}P_{T'}}{\mathrm{d}T'}$ indicates the temperature probability distribution function

ACPD
14, 17635–17679, 2014

(PDF), $\theta = 6132.9$ K. According to measurement-based analysis of Hoyle et al. (2005), δ_T can be linked to W_{sub}, $\delta_T \cong 4.3 W_{sub}$. Thus, we can find out the fraction of cirrus cloud, f_{hom}, where local $S_i(T')$ can exceed the homogeneous freezing saturation threshold S_{hom}.

2.5 Other ice nucleation parameterizations in CAM5

For comparison, BN and KL ice nucleation parameterizations are implemented in CAM5.3. The BN parameterization is derived from an approximation to the analytical solution of air parcel equations. This parameterization calculates the maximum ice saturation ratio and nucleated ice crystals number concentration explicitly in the rising air parcel and considers the competition between homogeneous and heterogeneous freezing (Barahona and Nenes, 2009). One advantage of BN parameterization is that the heterogeneous nucleation can be described by different nucleation spectrum, derived either from the classical nucleation theory (CNT) or from observations (e.g., Meyers et al., 1992; Phillips et al., 2008). In this work, the nucleation spectrum based on CNT is used to describe the immersion freezing on dust particles. Furthermore, the BN parameterization used in this study has been modified to consider the effects of PREICE by reducing the vertical velocity for ice nucleation (Barahona et al., 2013).

The KL parameterization is also implemented in CAM5.3. In this parameterization, the competition between different freezing mechanisms and the effects of PREICE are treated by explicitly calculating the evolution of S_i within one host-model's time step (e.g., 30 min). Compared to LP and BN parameterizations, this method is computationally more expensive. It is necessary to point out that, in the KL parameterization, the ice crystal number concentration produced via homogeneous freezing is not sensitive to the sulfate aerosol number concentration in most cases except for the highest ($4\,m\,s^{-1}$) updraft velocities (Fig. 4 and Table 1 in Kärcher and Lohmann, 2002a). As compared to the KL parameterization, the ice number concentrations from both BN and LP parameterizations are relatively more sensitive to sulfate aerosol number concentration (Fig. 9 in Barahona and Nenes, 2008; Fig. 2 in Liu and Penner, 2005).

ACPD
14, 17635–17679, 2014

We use the same diagnosed W_{sub} to drive LP, BN and KL parameterizations. The $W_{i,pre}$ is calculated using ice nucleation parameterization. Heterogeneous ice nucleation on dust particles is considered. All sulfate aerosol particles in the Aiken mode are used for the homogeneous nucleation. In LP and KL parameterizations, all dust in the coarse mode can act as IN. Thus, for consistency, the parameter that set an upper limiter on the freezing fraction of potential dust IN in the BN parameterization is set to 100 %. f_{hom} is also used for BN and KL parameterizations. Note that LP, BN and KL parameterizations are applied only for cirrus clouds. For mixed-phased clouds, we keep using the default heterogeneous nucleation formulations in CAM5.

2.6 Description of experiments

All simulations in this study have been carried out at $0.9^{\circ} \times 1.25^{\circ}$ horizontal resolution with 30 vertical levels and a 30 min time step, using prescribed present-day sea surface temperatures. Each experiment has a pair of simulations driven by present-day (the year of 2000) and pre-industrial (the year of 1850) aerosol and precursor emissions from Lamarque et al. (2010), separately. Without specification, we analyze present-day model results. All simulations are run for 6 years, and results from the last 5 years are used in the analysis.

All experiments are listed in Table 1. The Default, Preice, NoPreice and Nofhom experiments are used to evaluate the updates to the LP ice nucleation parameterization (Sect. 3). Compared to the Default experiment, the Preice experiment removes the two unphysical limiters (i.e., the lower size limiter of sulfate particles and the upper limiter of W_{sub}) used in default CAM5, while considering the effects of PREICE and the occurrence fraction of homogeneous freezing in cirrus clouds (f_{hom}). This experiment includes a combination of all our updates to the ice nucleation parameterization. Compared to the Preice experiment, NoPreice experiment is used to examine the effects of PREICE, and Nofhom experiment used to examine the effects of f_{hom}. The PreiceBN, NoPreiceBN, PreiceKL, and NoPreiceKL experiments are used to examine the PREICE effects in BN and KL ice nucleation parameterizations (Sect. 4). The Default, Pre-

ACPD
14, 17635–17679, 2014

ice, PreiceBN and PreiceKL experiments are used to compare the model performance among the three ice nucleation parameterizations (Sect. 5).

3 Model evaluations

First, we evaluate W_{sub} used for driving the ice nucleation parameterization and in-cloud N_i predicted by CAM5.3 with the default and updated ice nucleation parameterization. Aircraft measurements from the DOE Atmospheric Radiation Measurement Program (ARM)'s Small Particles in Cirrus (SPARTICUS) campaign (http://acrf-campaign.arm.gov/sparticus/) for the period of January to July 2010 are used to compare with model results. During the SPARTICUS campaign, ice crystal number and size distribution as well as ambient meteorological variables were routinely measured over the ARM Southern Great Plains (SGP) site (36.6° N, 97.5° W). Shattering of ice crystals was taken into account through uses of a new two-dimensional stereo-imaging probes (2-D-S) and improved algorithms (Lawson, 2011). To compare with the aircraft measurements, we sample instantaneous W_{sub} and N_i over the SGP site every three hours from model simulations for the period of January to July.

In the Default experiment, the upper limiter of W_{sub} is 0.2 m s^{-1}. Because the bin size is 0.06 m s^{-1}, there are no W_{sub} data larger than 0.24 m s^{-1} (Fig. 3, upper). However, aircraft measurements show that half ($\sim$ 55 %) of updraft velocity data surpasses 0.24 m s^{-1}. Thus, it is imperative to remove the upper limiter of W_{sub}. In other experiments without this upper limiter, the occurrence frequency of W_{sub} deceases with increasing W_{sub}, and agrees well with observation data (Fig. 3, upper). In the first smallest bin ($<$ 0.06 m s^{-1}), the modeled occurrence frequency of W_{sub} is less than observations. However, the influence of this difference on ice nucleation is small because ice nucleation events are significantly reduced in this lower updraft range ($<$ 0.06 m s^{-1}) due to the effect of PREICE (Fig. 6).

The most frequently observed N_i is in the range of 5–500 L^{-1} (Fig. 3, lower). The N_i from the Default experiment is mainly distributed in the range of 5–100 L^{-1}, and the

ACPD
14, 17635–17679, 2014

occurrence frequency of N_i at higher number concentrations ($> 100\,L^{-1}$) is significantly lower than observations. In the Preice experiment, ~ 11 % of N_i is higher than $100\,L^{-1}$, which is significantly larger than that in the Default experiment (~ 3 %). The main reason is that the Preice experiment removes the two unphysical limiters used for reducing the ice number concentrations. Although the occurrence frequency of $N_i > 100\,L^{-1}$ from the Preice experiment is still lower than observations (~ 30 %), its modeled histogram agrees better with the observations than the Default experiment. Compared to the Preice experiment, the occurrence frequency of $N_i > 100\,L^{-1}$ from the NoPreice experiment (~ 40 %) is increased significantly because the PREICE effect is not included to hinder the homogeneous freezing. The occurrence frequency of $N_i > 100\,L^{-1}$ from the Nofhom experiment (~ 22 %) is also lager than that from the Preice experiment because homogeneous nucleation takes place in the whole area of cirrus clouds in Nofhom.

The time scale of homogeneous freezing in a rising air parcel is a few minutes (140 s at $W = 0.1\,m\,s^{-1}$, Spichtinger and Krämer, 2013). It is still a challenge to sample the homogeneous freezing process and to grasp the fraction of cirrus clouds experiencing the homogeneous freezing in the real atmosphere. Thus, we cannot directly compare modeled f_{hom} with observations. Modeled f_{hom} from Sect. 2 peaks at the tropical tropopause layer (TTL) due to higher W_{sub} and lower T, with a maximum of 10–20 %. It is ~ 5 % at mid-latitudes, and even smaller at high latitudes. Here, we make a preliminary analysis of observed "upcoming" homogeneous nucleation events from the Tropical Composition, Cloud and Climate Coupling Experiment (TC4) and the Mid-latitude Airborne Cirrus Properties Experiment (MACPEX). An observed "upcoming" homogeneous nucleation event is defined as an event when S_i in a rising air parcel will reach S_{hom} within the time scale of one minute. The time scale of homogeneous freezing is assumed to be one minute because the observed "upcoming" homogeneous nucleation events usually go with high W ($> 0.5\,m\,s^{-1}$). The occurrence frequency of "upcoming" homogeneous nucleation events is 31 out of 8489 (3.7×10^{-3}) and 10 out of 27017 (3.7×10^{-4}) from TC4 and MACPEX in-cloud observation data, respectively. In other words, 3.7×10^{-3}

ACPD
14, 17635–17679, 2014

(TC4) and 3.7×10^{-4} (MACPEX) of cirrus clouds will go through homogeneous nucleation in one minute. With a time scale of 30 min (the model time step), the observed f_{hom} would be ~ 10 % and ~ 1 % over TC4 and MACPEX, respectively. Here, we assume the fraction of cirrus clouds that go through homogeneous nucleation is constant in every minute. Modeled f_{hom} is close to this observational analysis in the tropical regions. Both modeling and observational analyses suggest that f_{hom} in the tropical regions is larger than that in mid-latitudes. Diao et al. (2013) analyzed the evolution of ice crystals based on in-situ observations over North America. They found that ice crystal formation/growth is ~ 20 % of total analyzed samples. This value is not limited to the homogeneous freezing events, but includes the heterogeneous freezing and ice crystal growth events. So it is reasonable to assume that f_{hom} is less than 20 %.

Figure 4 compares the variation of modeled N_i vs. temperature against that observed in Krämer et al. (2009) who collected an extensive aircraft dataset in the temperature range of 183–250 K. Note that, these observations might be influenced by shattering of ice crystals, especially for warm cirrus clouds with relative larger ice crystals (Field et al., 2006). Therefore, for the following comparison, we should keep in mind that the observed N_i might be overestimated in warm cirrus clouds. The most distinct feature of this figure is that modeled N_i tends to increase with decreasing temperature for the whole temperature range. This temperature variation is caused by the homogeneous nucleation mechanism. Based on the same sulfate particles, homogeneous nucleation tends to produce more ice crystals at lower temperature (Liu and Penner, 2005). At temperature below 205 K, observed N_i is in the range of 10–80 L^{-1}, whereas modeled N_i is in the range of 50–2000 L^{-1}. Liu et al. (2012a) gave a possible explanation for this: heterogeneous nucleation could be the primary nucleation mechanism under these very low temperatures (i.e., near TTL) because homogeneous freezing might be suppressed by aerosols rich with organic matter (Murray, 2008; Krämer et al., 2009; Jensen et al., 2010; Murray et al., 2010). Barahona and Nenes (2011) suggested that small-scale temperature fluctuations could make cirrus clouds reside in a "dynamic equilibrium" state with sustained levels of low N_i consistent with cirrus char-

ACPD
14, 17635–17679, 2014

acteristics observed at TTL. Furthermore, Spichtinger and Krämer (2013) found that ice crystal production via homogeneous nucleation could be limited by high frequency gravity waves. However, these aerosol and dynamical characteristics are currently not accounted for in the model. In the temperature range of 205–230 K, modeled N_i is close to the observed values. The N_i from the Preice experiment is higher than that from the Default experiment, and agrees better with observations. The reason is the same as that for the PDF of N_i (Fig. 3, lower). Without the effects of PREICE, N_i from the NoPreice experiment is remarkably larger than the Preice experiment. Without considering f_{hom}, the Nofhom experiment produces higher N_i than the Preice experiment. Overall, the Preice experiment shows better agreement with observations in this temperature range as compared to the Default experiment.

The N_i differences between the default and updated nucleation schemes would affect modeled cloud radiative forcings. Figure 5 shows the annual and zonal means of longwave and shortwave cloud forcing (LWCF, SWCF), column-integrated cloud ice number concentration (CDNUMI), and ice water path (IWP). Modeled CDNUMI from the NoPreice experiment is significantly higher than those from other experiments. As a result, the NoPreice experiment predicts much higher IWP. Compared to the Preice experiment, the Nofhom experiment also produces more CDNUMI and thus higher IWP. Unlike cloud droplets in warm clouds, ice crystals in cirrus clouds have a significant influence on LWCF. Thus the NoPreice experiment predicts much stronger LWCF than other experiments, which is larger than observations in the tropical regions. LWCFs from Default, Preice and Nofhom experiments agree with observations in the tropical regions, but are underestimated at mid- and high latitudes. In all experiments, modeled SWCFs agree the observations at mid- and high latitudes, but are overestimated (more negative) in the tropical regions, especially for the NoPreice experiment. Overall, there is no remarkable difference between the Default and Preice experiments in cloud radiative forcings (both LWCF and SWCF) because the difference in CDNUMI is relatively small.

ACPD
14, 17635–17679, 2014

Table 2 gives global and annual means of cloud and radiative flux variables from present-day simulations in Table 1 and comparison with observations. Compared to the Default experiment, CDNUMI from the Preice, Nofhom and NoPreice experiments increases by 40 %, 133 %, and 1130 %, respectively. Because cirrus clouds can heat the atmosphere by absorbing and re-emitting the longwave terrestrial radiation (Liou, 1986), the increase in CDNUMI can lead to the increase of atmospheric stability and the weakening of convection, such as the fast atmospheric response discussed in Andrews et al. (2010). Thus, convective precipitation rates (PRECC) from Preice, Nofhom and NoPreice are reduced compared to the Default experiment, especially for the NoPreice experiment. Large-scale precipitation rates (PRECL) from the Default, Preice, Nofhom and NoPreice experiments are all close to each other (ranging from 1.04 to 1.05 mm day^{-1}). Compared to the Default experiment, IWP from Preice, Nofhom and NoPreice experiments increases by 1.23 g m^{-2}, 3.18 g m^{-2}, and 7.96 g m^{-2}, respectively. The reason is that higher ice number concentrations in these experiments lead to smaller ice crystal sizes and thus less sedimentation losses of ice water mass. In accordance with the increased ice water mass, high cloud fractions (CLDHGH) are also increased in Preice, Nofhom and NoPreice. Liquid water paths (LWP) and column-integrated droplet number concentration (CDNUMC) from Preice, Nofhom and NoPreice experiments are also increased with increasing CDNUMI. This might be a result of increased atmospheric stability and weakened convection. Obviously, SWCF and LWCF from Preice, Nofhom and NoPreice become stronger due to the increases in LWP, IWP, CDNUMC and CDNUMI as compared to the Default experiment. Changes in SWCF and LWCF between the Default and Preice experiments are moderate (−1.27 W m^{-2} in SWCF, 1.23 W m^{-2} in LWCF). Overall, global annual mean results from both the Default and Preice experiments show generally good agreements with observations.

The anthropogenic aerosol effects are given in Table 3. The more representative method suggested by Ghan (2013) is used to estimate aerosol effects on cloud radiative forcings. Cloud radiative forcings marked with an asterisk are diagnosed from the

ACPD
14, 17635–17679, 2014

whole-sky and clear-sky top-of-atmosphere radiative fluxes with aerosol scattering and absorption neglected. "Δ" indicates a change between present-day (the year 2000) and pre-industrial times (the year 1850) with the only change in aerosol and precursor gas emissions. ΔCDNUMI in the Preice experiment is larger than the Default experiment due to the use of all sulfate number concentration in the Aiken mode. The differences in cloud forcings (ΔSWCF* and ΔLWCF*) between Preice and Default experiments are less than standard deviations (0.19 W m^{-2} for ΔSWCF* and 0.13 W m^{-2} for ΔLWCF*) calculated from the difference of each of 5 years. ΔSWCF* and ΔLWCF* in the Nofhom experiment are both a little stronger than the Preice experiment. Because ΔCDNUMI is largest in the NoPreice experiment, this experiment gives the strongest changes in cloud forcings (ΔSWCF* and ΔLWCF*) and in cloud water paths (ΔLWP and ΔIWP). ΔPRECC in the Default, Preice and Nofhom experiments are negligibly small. Overall, the difference in the anthropogenic aerosol indirect forcing (ΔCF*) between the Default and Preice experiments is small (∼ 0.1 W m^{-2}).

4 PREICE effect and sensitivity to different ice nucleation parameterizations

In this section we analyze the effect of PREICE and its sensitivity to different ice nucleation parameterizations. Considering the PREICE effect, the effective updraft velocity, W_{eff}, which is used to drive the ice nucleation parameterization equals to W_{sub} minus $W_{\mathrm{i,pre}}$. Figure 6 shows the PDF of W_{sub}, W_{eff} and $W_{\mathrm{i,pre}}$ from homogeneous ice nucleation occurrence events in the Preice experiment. Results from PreiceBN and PreiceKL experiments have similar patterns to the Preice experiment (not shown). For ice nucleation occurrence events ($W_{\mathrm{eff}} > 0$), $W_{\mathrm{i,pre}}$ is mainly distributed in the range of 0–0.1 m s^{-1}. This indicates that ice nucleation usually happens at low PREICE number concentrations (< 50 L^{-1}). Different from the PDF pattern of model diagnosed W_{sub} (Fig. 3, upper) which includes all samples, the most frequently sampled W_{sub} for ice nucleation occurrence events is in the range of 0.1–0.4 m s^{-1} because W_{sub} must be

ACPD
14, 17635–17679, 2014

larger than $W_{i,pre}$. W_{eff} is mainly distributed in a range of 0–0.3 m s^{-1}, and rarely larger than 1.0 m s^{-1}. The comparison between W_{eff} and W_{sub} indicates that PREICE not only reduces the occurrence frequency of homogeneous nucleation, but also reduces the number density of nucleated ice crystals from homogeneous nucleation.

Figure 7 shows the annual zonal mean N_i from NoPreice and Preice experiments. NoPreiceBN, PreiceBN, NoPreiceKL and PreiceKL experiments are also analyzed. Because the effects of PREICE from experiments using BN and KL parameterization are similar (not shown), we only show the experiments using the LP parameterization here. Without the influence of PREICE, N_i is higher than 500 L^{-1} in the upper troposphere, and even higher (> 2000 L^{-1}) at mid- and high latitudes of the Southern Hemisphere (SH). After considering the PREICE effects, N_i is significantly reduced, especially at mid- and high latitudes in the upper troposphere (by a factor of ∼ 10). Global annual mean results show that, after considering the PREICE effects, CDNUMI from simulations using LP, BN and KL parameterizations is reduced by a factor of 6 ∼ 11 (Table 2). Thus, PREICE has a substantial influence on N_i. Compared to the distribution pattern from the NoPreice experiment, N_i from the Preice experiment is higher in the tropical tropopause region rather than in the SH upper troposphere. It seems that the influence of PREICE is relatively weaker in the tropical tropopause due to low T and high W_{sub} there (not shown).

Because of the large difference in N_i between experiments with and without the effects of PREICE, there must be resulting differences in cloud forcings and precipitation as explained above. Compared to experiments with the PREICE effect, PRECC from NoPreice, NoPreiceBN and NoPreiceKL experiments are reduced by 13 %, 10 %, and 15 %, respectively (Table 2). The change in SWCF is −11.1 W m^{-2}, −7.8 W m^{-2}, and −11.8 W m^{-2}, for simulations using the LP, BN and KL parameterization, respectively. The change in LWCF is 11.2 W m^{-2}, 8.0 W m^{-2}, and 12.6 W m^{-2}, respectively. Barahona et al. (2013) studied the effect of PREICE in GEOS5 with the BN parameterization. Change in LWCF and SWCF is 5 W m^{-2} and 4 W m^{-2}, respectively. In the ECHAM5 model with the KL parameterization, changes in LWCF and SWCF are

ACPD
14, 17635–17679, 2014

1.5 W m^{-2} and 0.95 W m^{-2}, respectively when heterogeneous nucleation and PREICE are taken into account (Kuebbeler et al., 2014). These differences in the effects of PREICE between different models can either be caused by the ice nucleation scheme itself or model input parameters (e.g., W_{sub}, RH_i and aerosol number concentration used to drive the ice nucleation parameterization).

Table 4 gives the influence of PREICE on the relative contribution of homogeneous vs. heterogeneous nucleation to the total ice number concentration in cirrus clouds. The contributions of heterogeneous nucleation from experiments without the effects of PREICE are less than 1 %. After considering the PREICE effects, the contribution of heterogeneous nucleation from Preice, PreiceBN, and PreiceKL experiments is increased to 17.6 %, 9.4 %, and 8.9 %, respectively. The reason is that, when PREICE is taken into account, the newly-formed ice crystals number concentration from homogeneous nucleation is significantly reduced (by a factor of ~ 10, not shown), whereas the ice crystals number concentration from heterogeneous nucleation is slightly decreased. This indicates that the PREICE effects can significantly change the relative contribution of homogeneous vs. heterogeneous nucleation to cirrus formation, especially at higher dust number concentrations (Table 4).

5 Comparison between different ice nucleation parameterizations

In this section we focus on the comparison between Default, Preice, PreiceBN and PreiceKL experiments. Because the two unphysical limiters are removed in Preice, PreiceBN and PreiceKL, N_i from these experiments are slightly larger than that from the Default experiment (Fig. 8, left). Furthermore, distribution patterns of N_i calculated by LP, BN and KL parameterizations are similar. One distinct feature of N_i distribution patterns from these experiments is that N_i is reduced in low-level cirrus. This is caused by the homogeneous nucleation rate reduction with increasing temperature (Koop, 2004). The global and annual mean CDNUMI from Preice, PreiceBN and PreiceKL experiments are close to each other (ranging from 116×10^6 to 119×10^6 m^{-2},

ACPD
14, 17635–17679, 2014

Table 2). However, differences in the global and annual mean percentage contribution from heterogeneous ice nucleation among Preice (17.6 %), PreiceBN (9.4 %) and PreiceKL (8.9 %) experiments are obvious (Table 4). Compared to BN and KL parameterizations, the LP parameterization includes a transition from the heterogeneous to homogeneous dominated regimes (Liu and Penner, 2005). In this transition regime, the newly-formed ice crystals come from both homogeneous and heterogeneous freezing, and the ice number concentration is a combination of heterogeneous nucleation and homogeneous nucleation contributions. This might be the reason for the higher heterogeneous nucleation contribution with the LP parameterization. Overall, the heterogeneous nucleation contributions from Preice, PreiceBN and PreiceKL experiments have similar distribution patterns (Fig. 8, right). Contribution from the heterogeneous nucleation is less than 10 % in the tropical upper troposphere and in the SH. In other words, homogeneous nucleation is the dominant contributor there. In the tropical lower troposphere and in the Northern Hemisphere (NH), heterogeneous nucleation became more important due to higher dust number concentrations. The study of Liu et al. (2012a) showed that difference in heterogeneous nucleation contribution between simulations using the LP parameterization and the BN parameterization is obvious, especially in the NH. Note that the empirical parameterization by Phillips et al. (2008) is used to describe the heterogeneous nucleation on dust particles for the BN parameterization in the work of Liu et al. (2012a), whereas the nucleation spectra based on CNT (without the upper limiter of dust activated fraction) is used in our study. Kuebbeler et al. (2014) also studied the contribution from heterogeneous nucleation using the ECHAM5 model with the KL parameterization. They found that heterogeneous nucleation contributes largest in the tropical troposphere and in the Arctic. At the mid- and high latitudes in the NH, their model results show that the contribution from heterogeneous nucleation is less than 1 %, whereas our model results show that the contribution from heterogeneous nucleation is larger than 10 %. One important difference between the KL parameterization used in our study and the KL parameterization used by Kuebbeler et al. (2014) is that they modified the KL parameterization by including an upper limiter of activated

ACPD
14, 17635–17679, 2014

fraction of pure dust particles as a function of S_i. This may cause the difference in the heterogeneous nucleation contribution between our and their studies.

Figure 9 shows the changes in annual and zonal means of LWCF, SWCF, CDNUMI and IWP between present-day minus pre-industrial times. ΔCDNUMI from all experiments are around zero in the SH because changes in sulfate and dust aerosol number densities that drive ice nucleation parameterizations are small. ΔCDNUMI from the PreiceKL experiment is smaller at mid–high latitudes in the NH as compared to other experiments. The reason is that the ice crystal number concentration from homogeneous freezing is not sensitive to sulfate number concentrations in most cases in the KL parameterization, whereas it is more sensitive to sulfate number concentrations in the other two parameterizations. However, ΔCDNUMI with the KL parameterization can reach 10×10^6 m^{-2} in the tropical regions due to low T and high W_{sub} there. Table 1 in Kärcher and Lohmann (2002a) showed that N_i became sensitive to sulfate number concentration under low temperature (200 K) and high updraft velocity (0.4 m s^{-1}, 4 m s^{-1}). Table 3 shows that the global mean ΔCDNUMI from the PreiceKL experiment (3.24×10^6 m^{-2}) is less than those from the Preice (8.46×10^6 m^{-2}) and PreiceBN experiments (5.62×10^6 m^{-2}). Compared to ΔCDNUMI, the fluctuation of ΔIWP is more complicated because many other microphysical processes (especially in mixed phase clouds) can impact ΔIWP. Overall, ΔIWP has a stronger variation in the NH, especially for Preice and PreiceKL experiments. At mid–high latitudes in the NH, ΔIWP from the Preice experiment is opposite to that from the PreiceKL experiment. Differences in global and annual mean ΔIWP among these experiments are also remarkable. Global mean ΔIWP from Preice, PreiceBN, and PreiceKL experiments are 0.12 g m^{-2}, 0.03 g m^{-2}, and 0.01 g m^{-2}, respectively (Table 3). ΔSWCF is mainly caused by aerosol indirect effects on warm clouds (Gettelman et al., 2012). Thus, patterns of ΔSWCF with different ice nucleation parameterizations are similar, and not obviously correlated with ΔCDNUMI. Differences in global and annual mean ΔSWCF* among Preice (−2.01 W m^{-2}), PreiceBN (−1.86 W m^{-2}) and PreiceKL (−1.88 W m^{-2}) are relatively small (Table 3). However, the patterns of ΔLWCF are associated with

ACPD
14, 17635–17679, 2014

those of ΔCDNUMI for all experiments. For example, both ΔLWCF and ΔCDNUMI from the PreiceKL experiment are negative at mid-latitudes in the NH. Table 3 shows that the global and annual mean ΔLWCF* is strongest in the Preice experiment (0.46 W m^{-2}), slightly weaker in PreiceBN (0.39 W m^{-2}), and weakest in the PreiceKL experiment (0.24 W m^{-2}). This is consistent with the difference in ΔCDNUMI.

6 Discussion and conclusions

One purpose of this study is to improve the representation of ice nucleation in CAM5. First, the PREICE effect is considered in CAM5.3 by reducing the vertical velocity used for driving the LP ice nucleation parameterization. The PREICE effect in the KL and BN parameterizations is treated by the same method. This is the main reason why the influence of PREICE simulated by LP, BN and KL parameterizations has similar patterns. Second, homogeneous freezing takes place spatially only in a portion of cirrus clouds rather than in the whole area of cirrus clouds. Barahona et al. (2013) considered a similar factor that accounts for ice nucleation occurrence area within the grid cell in GEOS5 based on results from a parcel statistical ensemble model (Barahona and Nenes, 2011). In our study, f_{hom} is diagnosed based on the empirical analysis of Kärcher and Burkhardt (2008) and Hoyle et al. (2005). The diagnosed f_{hom} is in general less than 20 % in consistent with the work of Diao et al. (2013). We note that the uncertainty caused by f_{hom} is moderate because the effect of f_{hom} on ice number concentration is weaker than the PREICE effect. Finally, the two unphysical limiters (the upper limiter of W_{sub} and the lower limiter for Aitken-mode sulfate aerosol size) used in the representation of ice nucleation in CAM5 are removed.

The diagnosed W_{sub} from the updated CAM5.3 model with the updraft limiter removed agrees well with SPARTICUS observations. Compared to the default model, both PDF of N_i and N_i variations with temperature from the updated model agree better with the observations in the temperature range of 205–230 K. At temperatures below 205 K, same as the default model, N_i predicted from the updated model is still

ACPD
14, 17635–17679, 2014

larger than observations. The difference in cloud radiative forcings between the updated model and the default model is moderate ($-1.27\,W\,m^{-2}$ in SWCF, $1.23\,W\,m^{-2}$ in LWCF). The aerosol LW indirect forcing ($\Delta LWCF^*$) from the update model ($0.46\,W\,m^{-2}$) is a little weaker than that from the default model ($0.51\,W\,m^{-2}$).

The influence of preexisting ice crystals is studied using the updated CAM5.3 model. Comparison among W_{sub}, W_{eff} and $W_{i,pre}$ indicates that PREICE not only reduces the occurrence frequency of homogeneous freezing, but also reduces the number density of nucleated ice crystals from homogeneous freezing. No matter which ice nucleation parameterization is used, modeled N_i is significantly reduced due to the PREICE effects, especially at mid- to high-latitudes in the upper troposphere (by a factor of ~ 10). Compared to the GEOS5 model using the BN parameterization and the ECHAM5 model using the KL parameterization, the influence of PREICE on cirrus cloud properties and cloud forcings is stronger in the updated CAM5.3 model. After considering the PREICE effects, the contribution of heterogeneous nucleation is significantly increased. Even if taking the PREICE effect into account, homogeneous freezing still produces $\sim 80\,\%$ of total ice crystals in cirrus clouds. However, heterogeneous nucleation produces $> 30\,\%$ of total ice crystals at the dust range of $10–100\,L^{-1}$, and heterogeneous nucleation becomes the dominant contributor ($> 80\,\%$) when dust number concentration is higher than $100\,L^{-1}$.

The comparison between different ice nucleation parameterizations is also investigated using the updated CAM5.3 model. Compared to LP and BN parameterizations, N_i from the KL parameterization is not sensitive to sulfate number concentrations. The global and annual mean change in column ice number concentration between present day and pre-industrial time ($\Delta CDNUMI$) with the KL parameterization ($3.24 \times 10^6\,m^{-2}$) is less that those with the LP parameterization ($8.46 \times 10^6\,m^{-2}$) and the BN parameterization ($5.62 \times 10^6\,m^{-2}$). The anthropogenic aerosols longwave indirect forcing $\Delta LWCF^*$ from the KL parameterization is $0.24\,W\,m^{-2}$, smaller than that from the LP ($0.46\,W\,m^{-2}$) and BN ($0.39\,W\,m^{-2}$) parameterizations. In the future, we will compare the sensitivity of N_i to sulfate number concentration as derived from ice nucleation parameterizations

ACPD
14, 17635–17679, 2014

to parcel model results under different environmental conditions (temperature, updraft and aerosol) to quantify the uncertainties of aerosol indirect effect on cirrus clouds.

The Supplement related to this article is available online at doi:10.5194/acpd-14-17635-2014-supplement.

Acknowledgements. X. Liu and K. Zhang were supported by the Office of Science of US Department of Energy as part of the Earth System Modeling Program. X. Shi would like to acknowledge the support from the National Natural Science Foundation of China (Grant No.41205071). We would like to acknowledge the use of computational resources (ark:/85065/d7wd3xhc) at the NCAR-Wyoming Supercomputing Center provided by the National Science Foundation and the State of Wyoming, and supported by NCAR's Computational and Information Systems Laboratory. PNNL is a multiprogram laboratory operated for DOE by Battelle Memorial Institute under contract DE-AC05-76RL01830.

References

Adler, R. F., Huffman, G. J., Chang, A., Ferraro, R., Xie, P.-P., Janowiak, J., Rudolf, B., Schneider, U., Curtis, S., Bolvin, D., Gruber, A., Susskind, J., Arkin, P., and Nelkin, E.: The Version-2 Global Precipitation Climatology Project (GPCP) monthly precipitation analysis (1979–present), J. Hydrometeorol., 4, 1147–1167, doi:10.1175/1525-7541(2003)004<1147:TVGPCP>2.0.CO;2, 2003.

Andrews, T., Forster, P. M., Boucher, O., Bellouin, N., and Jones, A.: Precipitation, radiative forcing and global temperature change, Geophys. Res. Lett., 37, L14701, doi:10.1029/2010GL043991, 2010.

Barahona, D. and Nenes, A.: Parameterization of cirrus cloud formation in large-scale models: homogeneous nucleation, J. Geophys. Res.-Atmos., 113, D11211, doi:10.1029/2007JD009355, 2008.

Barahona, D. and Nenes, A.: Parameterizing the competition between homogeneous and heterogeneous freezing in ice cloud formation – polydisperse ice nuclei, Atmos. Chem. Phys., 9, 5933–5948, doi:10.5194/acp-9-5933-2009, 2009.

ACPD
14, 17635–17679, 2014

Barahona, D. and Nenes, A.: Dynamical states of low temperature cirrus, Atmos. Chem. Phys., 11, 3757–3771, doi:10.5194/acp-11-3757-2011, 2011.
Barahona, D., Molod, A., Bacmeister, J., Nenes, A., Gettelman, A., Morrison, H., Phillips, V., and Eichmann, A.: Development of two-moment cloud microphysics for liquid and ice within the NASA Goddard earth observing system model (GEOS-5), Geosci. Model Dev. Discuss., 6, 5289–5373, doi:10.5194/gmdd-6-5289-2013, 2013.
Bretherton, C. S. and Park, S.: A new moist turbulence parameterization in the Community Atmosphere Model, J. Climate, 22, 3422–3448, doi:10.1175/2008JCLI2556.1, 2009.
Chen, T., Rossow, W. B., and Zhang, Y.: Radiative effects of cloud-type variations, J. Climate, 13, 264–286, doi:10.1175/1520-0442(2000)013<0264:REOCTV>2.0.CO;2, 2000.
Corti, T., Luo, B. P., Peter, T., Vomel, H., and Fu, Q.: Mean radiative energy balance and vertical mass fluxes in the equatorial upper troposphere and lower stratosphere, Geophys. Res. Lett., 32, L06802, doi:10.1029/2004GL021889, 2005.
Cziczo, D. J., Murphy, D. M., Hudson, P. K., and Thomson, D. S.: Single particle measurements of the chemical composition of cirrus ice residue during CRYSTAL-FACE, J. Geophys. Res.-Atmos., 109, D04201, doi:10.1029/2003jd004032, 2004.
Cziczo, D. J., Froyd, K. D., Hoose, C., Jensen, E. J., Diao, M., Zondlo, M. A., Smith, J. B., Twohy, C. H., and Murphy, D. M.: Clarifying the dominant sources and mechanisms of cirrus cloud formation, Science, 340, 1320–1324, doi:10.1126/science.1234145, 2013.
DeMott, P. J., Rogers, D. C., Kreidenweis, S. M., and Chen, Y. L.: Laboratory studies of ice nucleation by aerosol particles in upper tropospheric conditions, AIP Conf. Proc., 534, 451–454, doi:10.1063/1.1361904, 2000.
DeMott, P. J., Möhler, O., Stetzer, O., Vali, G., Levin, Z., Petters, M. D., Murakami, M., Leisner, T., Bundke, U., Klein, H., Kanji, Z. A., Cotton, R., Jones, H., Benz, S., Brinkmann, M., Rzesanke, D., Saathoff, H., Nicolet, M., Saito, A., Nillius, B., Bingemer, H., Abbatt, J., Ardon, K., Ganor, E., Georgakopoulos, D. G., and Saunders, C.: Resurgence in ice nuclei measurement research, B. Am. Meteorol. Soc., 92, 1623–1635, doi:10.1175/2011BAMS3119.1, 2011.
Diao, M., Zondlo, M. A., Heymsfield, A. J., Beaton, S. P., and Rogers, D. C.: Evolution of ice crystal regions on the microscale based on in situ observations, Geophys. Res. Lett., 40, 3473–3478, doi:10.1002/grl.50665, 2013.

ACPD
14, 17635–17679, 2014

Field, P. R., Heymsfield, A. J., and Bansemer, A.: Shattering and particle interarrival times measured by optical array probes in ice clouds, J. Atmos. Ocean. Tech., 23, 1357–1371, doi:10.1175/JTECH1922.1, 2006.

Fusina, F., Spichtinger, P., and Lohmann, U.: Impact of ice supersaturated regions and thin cirrus on radiation in the midlatitudes, J. Geophys. Res., 112, D24, doi:10.1029/2007jd008449, 2007.

Gettelman, A., Morrison, H., and Ghan, S. J.: A new two-moment bulk stratiform cloud microphysics scheme in the community atmosphere model, version 3 (CAM3). Part II: Single-column and global results, J. Climate, 21, 3660–3679, doi:10.1175/2008jcli2116.1, 2008.

Gettelman, A., Liu, X., Ghan, S. J., Morrison, H., Park, S., Conley, A. J., Klein, S. A., Boyle, J., Mitchell, D. L., and Li, J. L. F.: Global simulations of ice nucleation and ice supersaturation with an improved cloud scheme in the Community Atmosphere Model, J. Geophys. Res.-Atmos., 115, D18216, doi:10.1029/2009jd013797, 2010.

Gettelman, A., Liu, X., Barahona, D., Lohmann, U., and Chen, C.: Climate impacts of ice nucleation, J. Geophys. Res.-Atmos., 117, D20201, doi:10.1029/2012jd017950, 2012.

Ghan, S. J.: Technical Note: Estimating aerosol effects on cloud radiative forcing, Atmos. Chem. Phys., 13, 9971–9974, doi:10.5194/acp-13-9971-2013, 2013.

Greenwald, T. J., Stephens, G. L., Haar, T. H. V., and Jackson, D. L.: A physical retrieval of cloud liquid water over the global oceans using Special Sensor Microwave/Imager (SSM/I) observations, J. Geophys. Res., 98, 18471–18488, 1993.

Haag, W.: The impact of aerosols and gravity waves on cirrus clouds at midlatitudes, J. Geophys. Res., 109, D12202, doi:10.1029/2004JD004579, 2004.

Han, Q., Rossow, W. B., and Lacis, A. A.: Near-global survey of effective droplet radii in liquid water clouds using ISCCP data, J. Climate, 7, 465–497, doi:10.1175/1520-0442(1994)007<0465:NGSOED>2.0.CO;2, 1994.

Hendricks, J., Kärcher, B., and Lohmann, U.: Effects of ice nuclei on cirrus clouds in a global climate model, J. Geophys. Res.-Atmos., 116, D18206, doi:10.1029/2010JD015302, 2011.

Heymsfield, A. J., Miloshevich, L. M., Schmitt, C., Bansemer, A., Twohy, C., Poellot, M. R., Fridlind, A., and Gerber, H.: Homogeneous ice nucleation in subtropical and tropical convection and its influence on cirrus anvil microphysics, J. Atmos. Sci., 62, 41–64, doi:10.1175/JAS-3360.1, 2005.

ACPD
14, 17635–17679, 2014

Hoose, C. and Möhler, O.: Heterogeneous ice nucleation on atmospheric aerosols: a review of results from laboratory experiments, Atmos. Chem. Phys., 12, 9817–9854, doi:10.5194/acp-12-9817-2012, 2012.

Hoyle, C. R., Luo, B. P., and Peter, T.: The origin of high ice crystal number densities in cirrus clouds, J. Atmos. Sci., 62, 2568–2579, doi:10.1175/JAS3487.1, 2005.

IPCC: Climate Change 2007: The Physical Basis. Contribution of Working Group I to the Fourth Assessment Report of the Intergovernmental Panel on Climate Change, Cambridge Univ. Press, New York, 2007.

Jensen, E. J., Pfister, L., Bui, T.-P., Lawson, P., and Baumgardner, D.: Ice nucleation and cloud microphysical properties in tropical tropopause layer cirrus, Atmos. Chem. Phys., 10, 1369–1384, doi:10.5194/acp-10-1369-2010, 2010.

Jensen, E. J., Pfister, L., and Bui, T. P.: Physical processes controlling ice concentrations in cold cirrus near the tropical tropopause, J. Geophys. Res.-Atmos., 117, D11205, doi:10.1029/2011JD017319, 2012.

Jensen, E. J., Diskin, G., Lawson, R. P., Lance, S., Bui, T. P., Hlavka, D., McGill, M., Pfister, L., Toon, O. B., and Gao, R.: Ice nucleation and dehydration in the Tropical Tropopause Layer, P. Natl. Acad. Sci. USA, 110, 2041–2046, doi:10.1073/pnas.1217104110, 2013.

Kärcher, B. and Burkhardt, U.: A cirrus cloud scheme for general circulation models, Q. J. Roy. Meteor. Soc., 134, 1439–1461, doi:10.1002/qj.301, 2008.

Kärcher, B. and Lohmann, U.: A parameterization of cirrus cloud formation: homogeneous freezing of supercooled aerosols, J. Geophys. Res.-Atmos., 107, AAC 4–1-AAC 4–10, doi:10.1029/2001JD000470, 2002a.

Kärcher, B. and Lohmann, U.: A parameterization of cirrus cloud formation: homogeneous freezing including effects of aerosol size, J. Geophys. Res.-Atmos., 107, 4698, doi:10.1029/2001JD001429, 2002b.

Kärcher, B. and Lohmann, U.: A parameterization of cirrus cloud formation: heterogeneous freezing, J. Geophys. Res.-Atmos., 108, 4402, doi:10.1029/2002JD003220, 2003.

Kärcher, B., Hendricks, J., and Lohmann, U.: Physically based parameterization of cirrus cloud formation for use in global atmospheric models, J. Geophys. Res.-Atmos., 111, D01205, doi:10.1029/2005JD006219, 2006.

Kärcher, B., Möhler, O., DeMott, P. J., Pechtl, S., and Yu, F.: Insights into the role of soot aerosols in cirrus cloud formation, Atmos. Chem. Phys., 7, 4203–4227, doi:10.5194/acp-7-4203-2007, 2007.

ACPD
14, 17635–17679, 2014

Kay, J. E., Baker, M., and Hegg, D.: Microphysical and dynamical controls on cirrus cloud optical depth distributions, J. Geophys. Res.-Atmos., 111, D24205, doi:10.1029/2005jd006916, 2006.
Kiehl, J. T. and Trenberth, K. E.: Earth's annual global mean energy budget, B. Am. Meteorol. Soc., 78, 197–208, doi:10.1175/1520-0477(1997)078<0197:EAGMEB>2.0.CO;2, 1997.
Koop, T.: Homogeneous ice nucleation in water and aqueous solutions, Z. Phys. Chem., 218, 1231–1258, doi:10.1524/zpch.218.11.1231.50812, 2004.
Koop, T., Luo, B. P., Tsias, A., and Peter, T.: Water activity as the determinant for homogeneous ice nucleation in aqueous solutions, Nature, 406, 611–614, doi:10.1038/35020537, 2000.
Korolev, A. and Isaac, G. A.: Relative humidity in liquid, mixed-phase, and ice clouds, J. Atmos. Sci., 63, 2865–2880, doi:10.1175/JAS3784.1, 2006.
Krämer, M., Schiller, C., Afchine, A., Bauer, R., Gensch, I., Mangold, A., Schlicht, S., Spelten, N., Sitnikov, N., Borrmann, S., de Reus, M., and Spichtinger, P.: Ice supersaturations and cirrus cloud crystal numbers, Atmos. Chem. Phys., 9, 3505–3522, doi:10.5194/acp-9-3505-2009, 2009.
Kuebbeler, M., Lohmann, U., Hendricks, J., and Kärcher, B.: Dust ice nuclei effects on cirrus clouds, Atmos. Chem. Phys., 14, 3027–3046, doi:10.5194/acp-14-3027-2014, 2014.
Lamarque, J.-F., Bond, T. C., Eyring, V., Granier, C., Heil, A., Klimont, Z., Lee, D., Liousse, C., Mieville, A., Owen, B., Schultz, M. G., Shindell, D., Smith, S. J., Stehfest, E., Van Aardenne, J., Cooper, O. R., Kainuma, M., Mahowald, N., McConnell, J. R., Naik, V., Riahi, K., and van Vuuren, D. P.: Historical (1850–2000) gridded anthropogenic and biomass burning emissions of reactive gases and aerosols: methodology and application, Atmos. Chem. Phys., 10, 7017–7039, doi:10.5194/acp-10-7017-2010, 2010.
Lawson, R. P.: Effects of ice particles shattering on the 2D-S probe, Atmos. Meas. Tech., 4, 1361–1381, doi:10.5194/amt-4-1361-2011, 2011.
Li, J. L. F., Waliser, D. E., Chen, W. T., Guan, B., Kubar, T., Stephens, G., Ma, H. Y., Deng, M., Donner, L., Seman, C., and Horowitz, L.: An observationally based evaluation of cloud ice water in CMIP3 and CMIP5 GCMs and contemporary reanalyses using contemporary satellite data, J. Geophys. Res.-Atmos., 117, D16105, doi:10.1029/2012JD017640, 2012.
Liou, K. N.: Influence of cirrus clouds on weather and climate processes – a global perspective, Mon. Weather Rev., 114, 1167–1199, doi:10.1175/1520-0493(1986)114<1167:IOCCOW>2.0.CO;2, 1986.

ACPD
14, 17635–17679, 2014

Liu, X. H. and Penner, J. E.: Ice nucleation parameterization for global models, Meteorol. Z., 14, 499–514, doi:10.1127/0941-2948/2005/0059, 2005.
Liu, X., Penner, J. E., Ghan, S. J., and Wang, M.: Inclusion of ice microphysics in the NCAR Community Atmospheric Model Version 3 (CAM3), J. Climate, 20, 4526–4547, doi:10.1175/Jcli4264.1, 2007.
a !
Liu, X., Shi, X., Zhang, K., Jensen, E. J., Gettelman, A., Barahona, D., Nenes, A., and Lawson, P.: Sensitivity studies of dust ice nuclei effect on cirrus clouds with the Community Atmosphere Model CAM5, Atmos. Chem. Phys., 12, 12061–12079, doi:10.5194/acp-12-12061-2012, 2012a.
b !
Liu, X., Easter, R. C., Ghan, S. J., Zaveri, R., Rasch, P., Shi, X., Lamarque, J.-F., Gettelman, A., Morrison, H., Vitt, F., Conley, A., Park, S., Neale, R., Hannay, C., Ekman, A. M. L., Hess, P., Mahowald, N., Collins, W., Iacono, M. J., Bretherton, C. S., Flanner, M. G., and Mitchell, D.: Toward a minimal representation of aerosols in climate models: description and evaluation in the Community Atmosphere Model CAM5, Geosci. Model Dev., 5, 709–739, doi:10.5194/gmd-5-709-2012, 2012b.
Loeb, N. G., Wielicki, B. A., Doelling, D. R., Smith, G. L., Keyes, D. F., Kato, S., Manalo-Smith, N., and Wong, T.: Toward optimal closure of the earth's top-of-atmosphere radiation budget, J. Climate, 22, 748–766, doi:10.1175/2008JCLI2637.1, 2009.
Lohmann, U. and Feichter, J.: Global indirect aerosol effects: a review, Atmos. Chem. Phys., 5, 715–737, doi:10.5194/acp-5-715-2005, 2005.
Lohmann, U., Spichtinger, P., Jess, S., Peter, T., and Smit, H.: Cirrus cloud formation and ice supersaturated regions in a global climate model, Environ. Res. Lett., 3, 045022(11p), doi:10.1088/1748-9326/3/4/045022, 2008.
Meyers, M. P., Demott, P. J., and Cotton, W. R.: New primary ice-nucleation parameterizations in an explicit cloud model, J. Appl. Meteorol., 31, 708–721, doi:10.1175/1520-0450(1992)031<0708:NPINPI>2.0.CO;2, 1992.
Morrison, H. and Gettelman, A.: A new two-moment bulk stratiform cloud microphysics scheme in the Community Atmosphere Model, Version 3 (CAM3). Part I: Description and numerical tests, J. Climate, 21, 3642–3659, doi:10.1175/2008jcli2105.1, 2008.
Murray, B. J.: Inhibition of ice crystallisation in highly viscous aqueous organic acid droplets, Atmos. Chem. Phys., 8, 5423–5433, doi:10.5194/acp-8-5423-2008, 2008.

ACPD
14, 17635–17679, 2014

Murray, B. J., Wilson, T. W., Dobbie, S., Cui, Z., Al-Jumur, S. M. R. K., Möhler, O., Schnaiter, M., Wagner, R., Benz, S., Niemand, M., Saathoff, H., Ebert, V., Wagner, S., and Kärcher, B.: Heterogeneous nucleation of ice particles on glassy aerosols under cirrus conditions, Nat. Geosci., 3, 233–236, doi:10.1038/ngeo817, 2010.

Neale, R. B., Gettelman, A., Park, S., Conley, A. J., Kinnison, D., Marsh, D., Smith, A. K., Vitt, F., Morrison, H., Cameron-Smith, P., Collins, W. D., Iacono, M. J., Easter, R. C., Liu, X., and Taylor, M. A.: Description of the NCAR Community Atmosphere Model (CAM 5.0), NCAR Tech. Note NCAR/TN-485+STR, 289 pp., Natl. Cent. for Atmos. Res, Boulder, Co, 2012.

Phillips, V. T. J., DeMott, P. J., and Andronache, C.: An empirical parameterization of heterogeneous ice nucleation for multiple chemical species of aerosol, J. Atmos. Sci., 65, 2757–2783, doi:10.1175/2007jas2546.1, 2008.

Platnick, S., King, M. D., Ackerman, S. A., Menzel, W. P., Baum, B. A., Riedi, J. C., and Frey, R. A.: The MODIS cloud products: algorithms and examples from Terra, IEEE T. Geosci. Remote, 41, 459–473, doi:10.1109/TGRS.2002.808301, 2003.

Pruppacher, H. R. and Klett, J. D.: Microphysics of Cloud and Precipitation, Springer, New York, 954 pp., 1997.

Rossow, W. B. and Schiffer, R. A.: Advances in understanding clouds from ISCCP, B. Am. Meteorol. Soc., 80, 2261–2287, doi:10.1175/1520-0477(1999)080<2261:AIUCFI>2.0.CO;2, 1999.

Salzmann, M., Ming, Y., Golaz, J.-C., Ginoux, P. A., Morrison, H., Gettelman, A., Krämer, M., and Donner, L. J.: Two-moment bulk stratiform cloud microphysics in the GFDL AM3 GCM: description, evaluation, and sensitivity tests, Atmos. Chem. Phys., 10, 8037–8064, doi:10.5194/acp-10-8037-2010, 2010.

Shi, X., Wang, B., Liu, X., and Wang, M.: Two-moment bulk stratiform cloud microphysics in the grid-point atmospheric model of IAP LASG (GAMIL), Adv. Atmos. Sci., 30, 868–883, doi:10.1007/s00376-012-2072-1, 2013.

Spichtinger, P. and Gierens, K. M.: Modelling of cirrus clouds – Part 2: Competition of different nucleation mechanisms, Atmos. Chem. Phys., 9, 2319–2334, doi:10.5194/acp-9-2319-2009, 2009.

Spichtinger, P. and Krämer, M.: Tropical tropopause ice clouds: a dynamic approach to the mystery of low crystal numbers, Atmos. Chem. Phys., 13, 9801–9818, doi:10.5194/acp-13-9801-2013, 2013.

ACPD
14, 17635–17679, 2014

Szyrmer, W. and Zawadzki, I.: Biogenic and anthropogenic sources of ice-forming nuclei: a review, B. Am. Meteorol. Soc., 78, 209–228, doi:10.1175/1520-0477(1997)078<0209:BAASOI>2.0.CO;2, 1997.

Wang, M. and Penner, J. E.: Cirrus clouds in a global climate model with a statistical cirrus cloud scheme, Atmos. Chem. Phys., 10, 5449–5474, doi:10.5194/acp-10-5449-2010, 2010.

Wang, P.-H., Minnis, P., McCormick, M. P., Kent, G. S., Yue, G. K., Young, D. F., and Skeens, K. M.: A 6-year climatology of cloud occurence frequency from Stratospheric Aerosol and Gas Experiment II observations (1985–1990), J. Geophys. Res., 101, 407–429, doi:10.1029/96JD01780, 1996.

Weng, F. Z. and Grody, N. C.: Retrieval of cloud liquid water using the Special Sensor Microwave Imager (SSM/I), J. Geophys. Res., 99, 25535–25551, 1994.

Wielicki, B. A., Barkstrom, B. R., Harrison, E. F., Lee, R. B., Louis Smith, G., and Cooper, J. E.: Clouds and the Earth's Radiant Energy System (CERES): An Earth Observing System Experiment, B. Am. Meteorol. Soc., 77, 853–868, doi:10.1175/1520-0477(1996)077<0853:CATERE>2.0.CO;2, 1996.

Wylie, D. P. and Menzel, W. P.: Eight years of high cloud statistics using HIRS, J. Climate, 12, 170–184, doi:10.1175/1520-0442-12.1.170, 1999.

Wylie, D., Jackson, D. L., Menzel, W. P., and Bates, J. J.: Trends in global cloud cover in two decades of HIRS observations, J. Climate, 18, 3021–3031, doi:10.1175/JCLI3461.1, 2005.

Zhang, K., Liu, X., Wang, M., Comstock, J. M., Mitchell, D. L., Mishra, S., and Mace, G. G.: Evaluating and constraining ice cloud parameterizations in CAM5 using aircraft measurements from the SPARTICUS campaign, Atmos. Chem. Phys., 13, 4963–4982, doi:10.5194/acp-13-4963-2013, 2013a.

Zhang, K., Liu, X., Comstock, J., Wang, M., Wan, H., and Bui, T.: Vertical Draft Velocity in Cirrus Clouds and Long-Wave Aerosol Indirect Effect, The Atmosphere Model Working Group Meeting, Boulder, Colo., 11–13 February 2013, 2013b.

ACPD
14, 17635–17679, 2014

Table 1. List of experiments conducted in this study.

Experiment	Two limiter	PREICE	f_{hom}	Ice parameterization
Default	Yes	No	No	LP
Preice	No	Yes	Yes	LP
NoPreice	No	No	Yes	LP
Nofhom	No	Yes	No	LP
PreiceBN	No	Yes	Yes	BN
NoPreiceBN	No	No	Yes	BN
PreiceKL	No	Yes	Yes	KL
NoPreiceKL	No	No	Yes	KL

ACPD
14, 17635–17679, 2014

Table 2. Global annual mean results from present-day simulations and observations. Shown are total cloud fraction (CLDTOT,%) and high cloud fraction (CLDHGH,%) compared to ISCCP data (Rossow and Schiffer, 1999), MODIS data (Platnick et al., 2003), and HIRS data (Wylie et al., 2005), shortwave cloud forcing (SWCF, $W\,m^{-2}$), longwave cloud forcing (LWCF, $W\,m^{-2}$), whole-sky shortwave (FSNT, $W\,m^{-2}$) and longwave (FLNT, $W\,m^{-2}$) net radiative fluxes at the top of the atmosphere, clear-sky shortwave (FSNTC, $W\,m^{-2}$) and longwave (FLNTC, $W\,m^{-2}$) radiative fluxes at the top of the atmosphere compared to ERBE data (Kiehl and Trenberth, 1997) and CERES data (Loeb et al., 2009), liquid water path (LWP, $g\,m^{-2}$) compared to SSM/I oceans data (Greenwald et al., 1993; Weng and Grody, 1994) and ISCCP data (Han et al., 1994), ice water path (IWP, $g\,m^{-2}$) compared to CloudSat data (Li et al., 2012), column-integrated grid-mean cloud droplet number concentration (CDNUMC, $10^{10}\,m^{-2}$) compared to MODIS data (Table 4 in Barahona et al., 2013), column-integrated grid-mean ice crystal number concentration (CDNUMI, $10^{6}\,m^{-2}$), convective (PRECC, $mm\,day^{-1}$) and large-scale (PRECL, $mm\,day^{-1}$) and total precipitation rate (PRECT, $mm\,day^{-1}$) compared to Global Precipitation Climatology Project data set (Adler et al., 2003).

	Default	Preice	Nofhom	NoPreice	PreiceBN	NoPreiceBN	PreiceKL	NoPreiceKL	OBS
CLDTOT	62.52	63.01	64.37	67.95	63.45	67.30	63.49	68.92	62–75
CLDHGH	36.34	37.26	38.92	44.12	37.95	43.55	38.01	45.89	21–33
SWCF	−50.25	−51.52	−53.96	−62.67	−51.30	−59.07	−51.38	−63.15	−(46–53)
LWCF	22.42	23.65	27.12	34.81	23.38	31.42	23.25	35.85	27–31
FSNT	237.38	236.08	233.66	225.16	236.33	228.71	236.21	224.74	234–242
FLNT	−236.26	−234.88	−231.44	−222.49	−235.24	−226.38	−235.32	−221.50	−(234–240)
FSNTC	287.67	287.63	287.67	287.88	287.66	287.83	287.62	287.94	287–288
FLNTC	−258.68	−258.53	−258.57	−257.31	−258.62	−257.80	−258.57	−257.34	−(265–269)
LWP	43.62	43.90	44.60	46.72	43.84	45.88	43.94	46.78	50–87
IWP	16.37	17.60	19.55	24.33	17.09	21.09	17.01	23.87	25.8
CDNUMC	1.37	1.39	1.42	1.53	1.39	1.49	1.40	1.53	1.96
CDNUMI	83.20	119.32	193.30	1021.05	116.19	702.59	119.43	1267.13	
PRECC	2.01	1.97	1.90	1.71	1.98	1.78	1.98	1.69	
PRECL	1.04	1.05	1.05	1.05	1.05	1.06	1.05	1.05	
PRECT	3.05	3.02	2.95	2.75	3.02	2.84	3.03	2.74	2.68

ACPD
14, 17635–17679, 2014

Table 3. Global annual mean variables changes (present-day minus pre-industrial times). Illustrated are changes in net cloud forcing (ΔCF*, W m^{-2}) as well as the long-wave (ΔLWCF*, W m^{-2}) and shortwave (ΔSWCF*, W m^{-2}) components, the changes in convective (ΔPRECC, mm day^{-1}), large-scale (ΔPRECL, mm day^{-1}) and total precipitation rate (ΔPRECT, mm day^{-1}), the change in total cloud fraction (ΔCLDTOT, %), high cloud fraction (ΔCLDHGH, %), liquid water path (ΔLWP, g m^{-2}), ice water path (ΔIWP, g m^{-2}), and column droplet number concentration (ΔCDNUMC, 10^{10} m^{-2}), and column ice number concentration (ΔCDNUMI, 10^{6} m^{-2}).

	Default	Preice	Nofhom	NoPreice	PreiceBN	NoPreiceBN	PreiceKL	NoPreiceKL
ΔCF*	−1.44	−1.55	−1.60	−2.14	−1.47	−1.88	−1.64	−2.23
ΔSWCF*	−1.95	−2.01	−2.13	−4.51	−1.86	−3.58	−1.88	−3.94
ΔLWCF*	0.51	0.46	0.53	2.37	0.39	1.70	0.24	1.71
ΔPRECC	0	0	0	−0.03	−0.01	−0.02	0	−0.02
ΔPRECL	−0.0	−0.01	−0.01	−0.02	−0.01	−0.02	−0.01	−0.02
ΔPRECT	−0.01	−0.01	−0.01	−0.05	−0.02	−0.04	−0.01	−0.04
ΔCLDTOT	0.22	0.28	0.40	0.84	0.32	0.70	0.19	0.74
ΔCLDHGH	0.02	0.20	0.24	0.95	0.12	0.73	0.01	0.62
ΔLWP	3.83	3.59	3.77	5.73	3.40	4.33	3.66	4.56
ΔIWP	0.12	0.12	0.14	1.21	0.03	0.62	0.01	0.60
ΔCDNUMC	0.38	0.38	0.40	0.47	0.38	0.44	0.39	0.45
ΔCDNUMI	5.60	8.46	13.10	327.38	5.62	116.49	3.24	225.42

ACPD
14, 17635–17679, 2014

Table 4. All percentage contributions from heterogeneous ice nucleation to total ice crystal number concentration (in unit of %) within different ranges of dust number concentration for all present-day simulations. Model results are sampled every three hours. Only ice nucleation occurrence events are analyzed.

Dust range	Default	Preice	Nofhom	NoPreice	PreiceBN	NoPreiceBN	PreiceKL	NoPreiceKL
1–10 L^{-1}	6.8	5.7	2.1	0.1	3.3	0.3	3.4	0.1
10–100 L^{-1}	62.1	41.2	21.0	1.4	34.8	3.9	33.8	1.9
> 100 L^{-1}	99.5	89.8	78.0	10.9	92.2	39.2	93.0	25.8
All	27.9	17.6	6.7	0.5	9.4	1.0	8.9	0.5

ACPD
14, 17635–17679, 2014

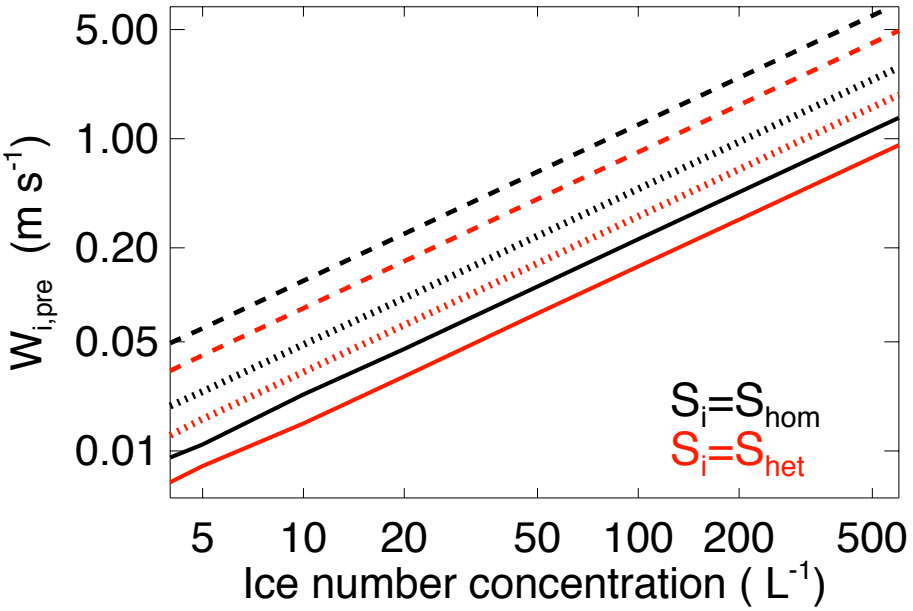

Figure 1. Vertical velocity reduction caused by PREICE ($W_{i,pre}$) as a function of ice number concentration. Results are shown for different ice radius, 10 µm (solid line), 25 µm (dotted line) and 50 µm (dash line). The ambient condition is that T = −60 °C, P = 230 hpa, S_i = S_{het} (red) and S_i = S_{hom} (black).

ACPD
14, 17635–17679, 2014

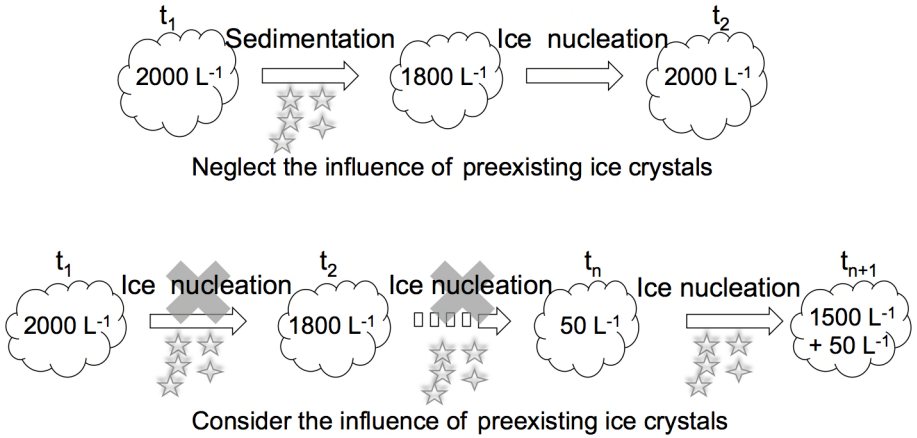

Figure 2. Schematic diagram of cirrus cloud evolution. Upper panel represents the default ice nucleation scheme that neglects the influence of PREICE, lower panel represents the updated scheme that considers the PREICE effect. The ambient environmental condition is assumed to be constant in-between time steps. Heterogeneous nucleation is not taken into account.

ACPD
14, 17635–17679, 2014

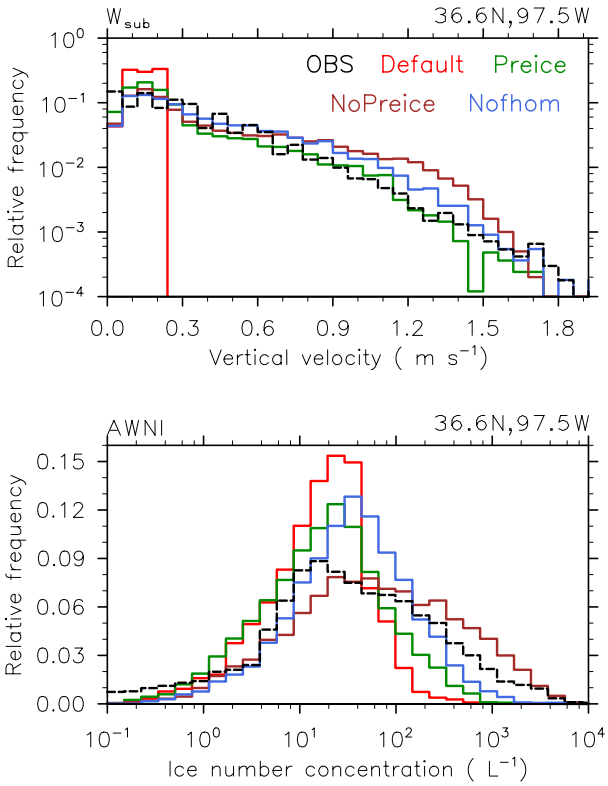

Figure 3. Probability distribution frequency of sub-grid updraft velocity (W_{sub}, upper) and in-cloud ice number concentration (N_i, lower) for Default, Preice, Nofhom and NoPreice experiments. Black-dashed line refers to aircraft measurements from the SPARTICUS campaign. The observed W_{sub} data was averaged over 50 km by 50 km grid (Zhang et al., 2013b). Model results are sampled over the field measurement site every three hours.

ACPD
14, 17635–17679, 2014

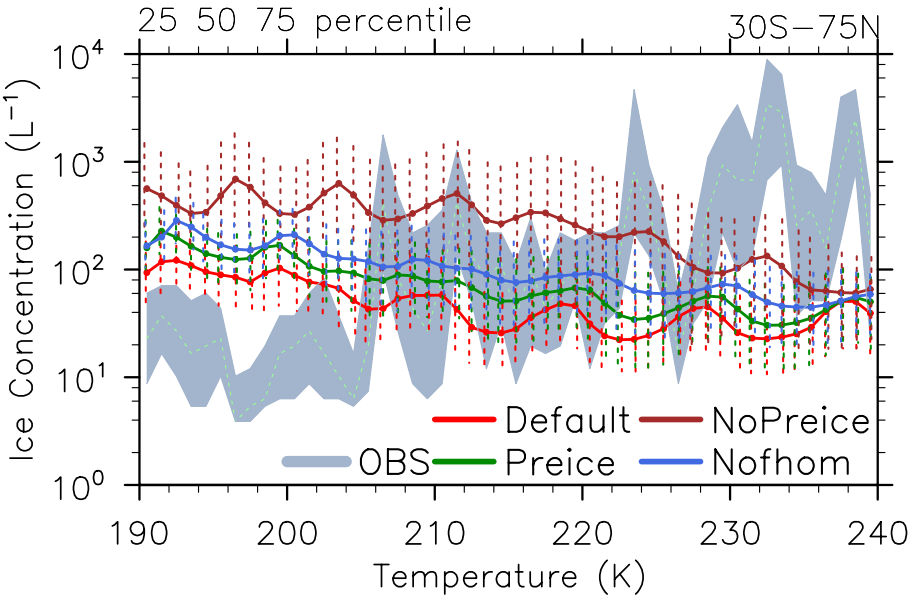

Figure 4. In-cloud ice crystal number concentration (N_i, L^{-1}) vs. temperature for Default, Preice, Nofhom and NoPreice experiments. Model results are sampled every three hours over tropical, mid-latitude and Arctic regions including the observation locations reported in Krämer et al. (2009). The 50 % percentile (solid line), 25 % and 75 % percentiles (error bar) are shown for each 1 K temperature bin. The gray color indicates observations between 25 % and 75 % percentiles.

ACPD
14, 17635–17679, 2014

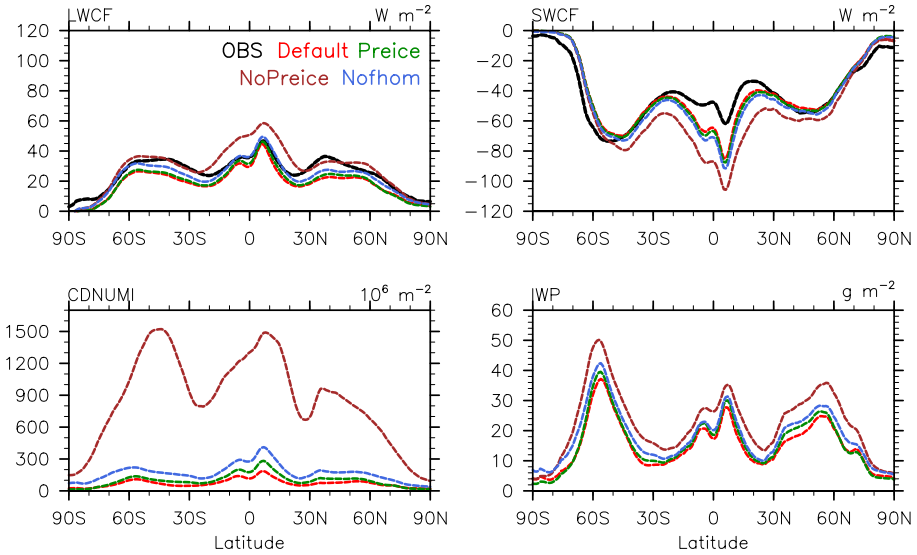

Figure 5. Annual and zonal mean distributions of longwave and shortwave cloud forcing (SWCF, LWCF), column cloud ice number concentration (CDNUMI), and ice water path (IWP). Black-solid line refers to CERES data for cloud forcing (Wielicki et al., 1996). Units are shown in the upper right corner.

ACPD
14, 17635–17679, 2014

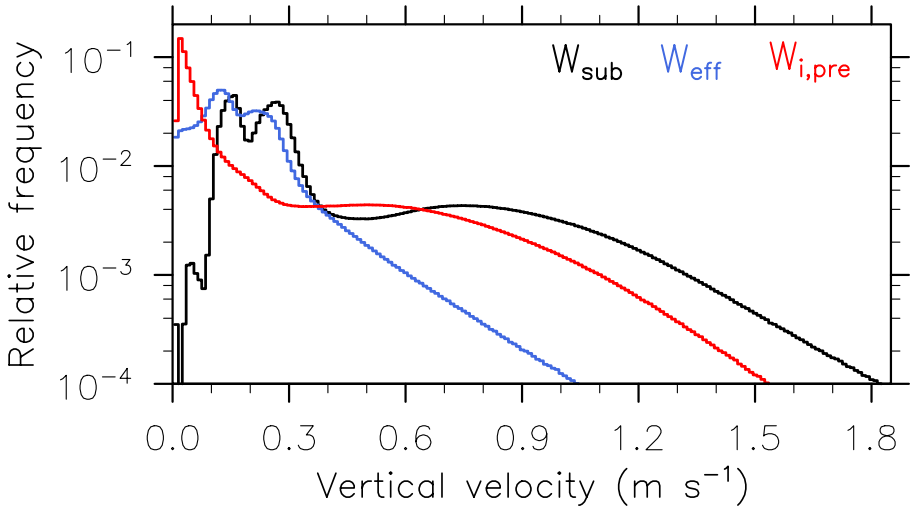

Figure 6. Probability distribution frequency (PDF) of sub-grid updraft velocity (W_{sub}, black), effective updraft velocity (W_{eff}, blue) and vertical velocity reduction caused by PREICE ($W_{i,pre}$, red) from the Preice experiment. Model results are sampled every three hours. Only homogeneous ice nucleation occurrence events ($W_{eff} > 0$) are analyzed.

ACPD
14, 17635–17679, 2014

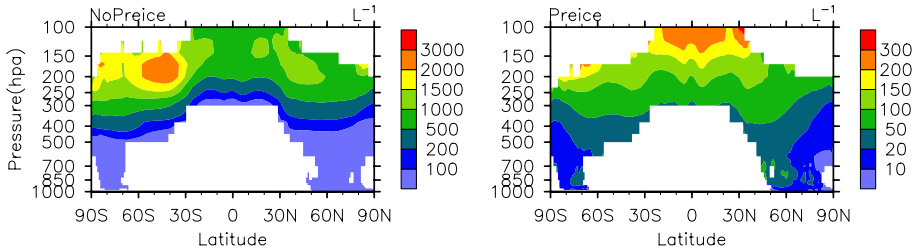

Figure 7. Annual zonal mean in-cloud ice crystal number concentration (N_i, L^{-1}) from NoPreice (left) and Preice (right) experiments. Note the different color bars. Results are sampled from model grids where annual mean occurrence frequency of ice nucleation events is greater than 0.001.

ACPD
14, 17635–17679, 2014

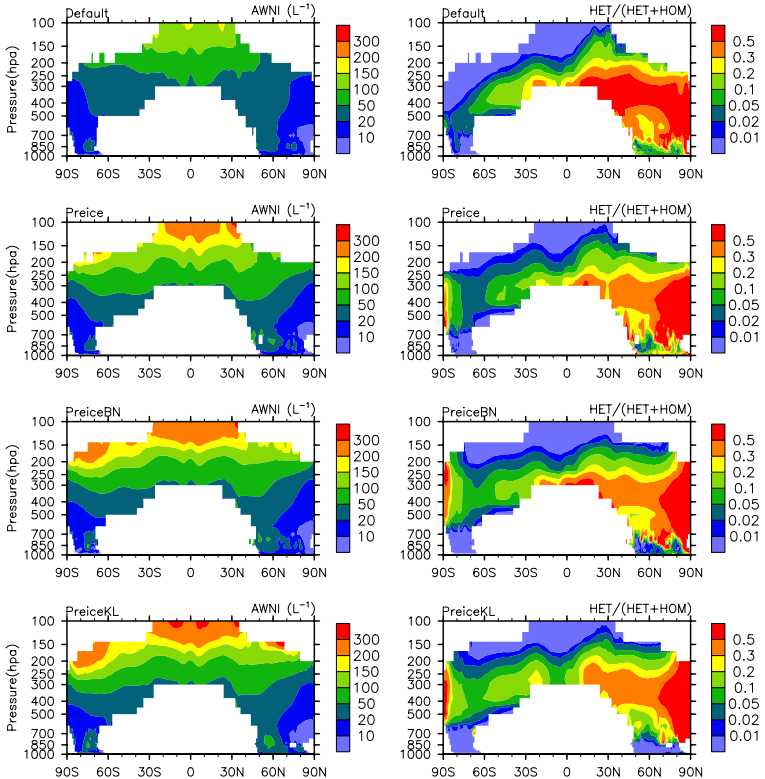

Figure 8. Same as Fig. 7, but for in-cloud ice crystal number concentration (L^{-1}, left) and percentage contribution from heterogeneous ice nucleation to total ice crystal number concentration (%, right) from Default, Preice, PreiceBN and PreiceKL experiments.

ACPD
14, 17635–17679, 2014

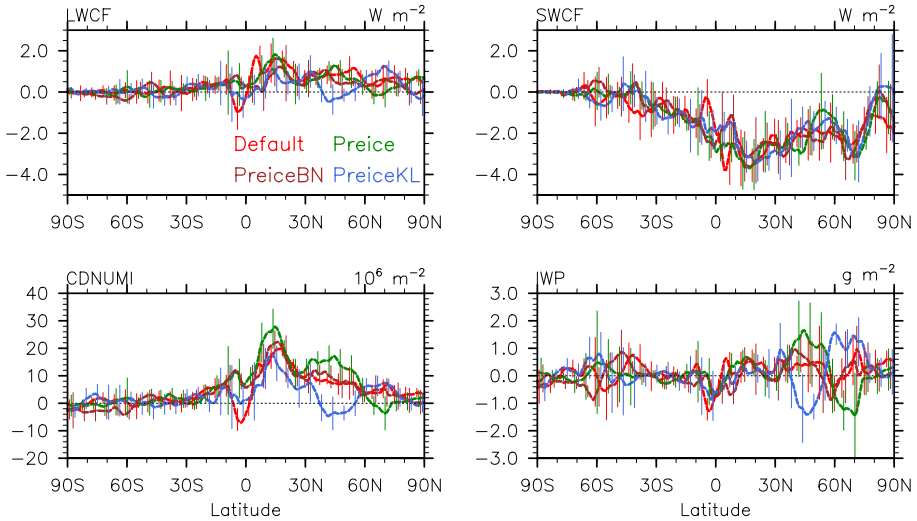

Figure 9. Changes (present-day minus pre-industrial times) in annual and zonal mean distributions of longwave and shortwave cloud forcing (LWCF, SWCF), column cloud ice number concentration (CDNUMI), and ice water path (IWP) for Default, Preice, PreiceBN and PreiceKL experiments. The vertical bars overloading on solid lines indicate the ranges of two standard deviation calculated from the difference of each of 5 years at different latitudes.

ACPD
14, 17635–17679, 2014